molecules

MDPI

Article

Luminescent Properties and Charge Compensator Effects of $SrMo_{0.5}W_{0.5}O_4$:Eu^{3+} for White Light LEDs

Li Kong [1], Hao Sun [1], Yuhao Nie [1], Yue Yan [1], Runze Wang [1], Qin Ding [1], Shuang Zhang [1], Haihui Yu [2,*] and Guoyan Luan [1]

[1] Institute of Petrochemical Technology, Jilin Institute of Chemical Technology, Jilin 132022, China
[2] School of Chemical Engineering, Northeast Electric Power University, Jilin 132012, China
* Correspondence: hhyu@neepu.edu.cn

Abstract: The high-temperature solid-phase approach was used to synthesize Eu^{3+}-doped $SrMo_{0.5}W_{0.5}O_4$ phosphors, whose morphological structure and luminescence properties were then characterized by XRD, SEM, FT-IR, excitation spectra, emission spectra, and fluorescence decay curves. The results reveal that the best phosphor synthesis temperature was 900 °C and that the doping of Eu^{3+} and charge compensators (K^+, Li^+, Na^+, NH_4^+) had no effect on the crystal phase change. $SrMo_{0.5}W_{0.5}O_4$:Eu^{3+} has major excitation peaks at 273 nm, 397 nm, and 464 nm, and a main emission peak at 615 nm, making it a potential red fluorescent material to be used as a down converter in UV LEDs (273 nm and 397 nm) and blue light LEDs (464 nm) to achieve Red emission. The emission spectra of $Sr_{1-y}Mo_{0.5}W_{0.5}O_4$:y$Eu^{3+}$(y = 0.005, 0.01, 0.02, 0.05, 0.07) excited at 273 were depicted, with the Eu^{3+} concentration increasing the luminescence intensity first increases and then decreases, the emission peak intensity of $SrMo_{0.5}W_{0.5}O_4$:Eu^{3+} achieves its maximum when the doping concentration of Eu^{3+} is 1%, and the critical transfer distance is calculated as 25.57 Å. When various charge compensators such as K^+, Li^+, Na^+, and NH_4^+ are added to $SrMo_{0.5}W_{0.5}O_4$:Eu^{3+}, the NH_4^+ shows the best effect with the optimal doping concentration of 3wt%. The $SrMo_{0.5}W_{0.5}O_4$:Eu^{3+},NH_4^+ color coordinate is (0.656,0.343), which is close to that of the ideal red light (0.670,0.333).

Keywords: $SrMo_{0.5}W_{0.5}O_4$:Eu^{3+}; charge compensator; Luminescence performance; w-LED

check for updates

Citation: Kong, L.; Sun, H.; Nie, Y.; Yan, Y.; Wang, R.; Ding, Q.; Zhang, S.; Yu, H.; Luan, G. Luminescent Properties and Charge Compensator Effects of $SrMo_{0.5}W_{0.5}O_4$:Eu^{3+} for White Light LEDs. *Molecules* **2023**, *28*, 2681. https://doi.org/10.3390/molecules28062681

Academic Editors: Andrei S. Potapov, Vladislava V. Matveevskaya, Carlos D.S. Brites and Fernando Baiao Dias

Received: 10 January 2023
Revised: 12 March 2023
Accepted: 13 March 2023
Published: 16 March 2023

1. Introduction

As a new generation of the light source of solid-state lighting, white light-emitting diodes (hereafter referred to as the white light LEDs, w-LEDs, etc.) have piqued the interest of scholars both at home and abroad for their high efficiency, energy savings, and environmental protection advantages [1–4]. The white light LED used to be created by combining a GaN chip that emits blue light with yellow phosphors (YAG:Ce^{3+}) that can be effectively excited by blue light [5]. However, this approach typically generates a low color rendering index because of the lack of red light in the emission spectrum of the yellow phosphor. The solution is to add red phosphors that can be efficiently excited by blue light [6,7] or use the high-efficiency UV LED and the phosphors that can be excited by it [8,9]. As a result, it is critical to investigate red phosphors that can be successfully stimulated by blue light and UV light.

It is well known that Eu^{3+} is an outstanding rare earth ion generating red light and can be effectively stimulated by blue light and UV light [10–14]. For instance, a new red phosphor Sr_3NaSbO_6:Eu^{3+} doped with Eu^{3+} was developed, and its emission spectra under excitation at 285 nm is located 500–700 nm, with the primary peak at 618 nm, indicating that this phosphor is a red phosphor that can be successfully stimulated by UV light [15]. $Li_{2.06}Nb_{0.18}Ti_{0.76}O_3$:$Eu^{3+}$ phosphors by sol-gel method were prepared. When the doping proportion of Eu^{3+} is x = 3 wt%, the primary excitation peak is at 396 nm, the central emission peak is at 612 nm, and its color coordinate is better than the commercial red

phosphor Y_2O_3:Eu^{3+} [16]. The phosphors Y_2SiO_5:Eu^{3+} synthesized by the solid-state reaction method can be effectively excited by near-UV (394 nm), and the major peak is located at 611 nm, the critical quenching concentration of Eu^{3+} in the phosphor is determined to be 15 mol%, and the critical transfer distance is calculated as 8.90 Å; co-doping Y_2SiO_5:Eu^{3+} with Ge^{4+} helps to improve the luminescence intensity and color purity, it can be concluded that efficient red light emitting diodes were fabricated using Ge^{4+}, Eu^{3+} co-doped phosphor based on near ultraviolet(NUV) excited LED lights [17]. By using a high-temperature solid-phase reaction, a new lithium salt type $NaBaBi_2(PO_4)_3$:Eu^{3+} phosphor was synthesized, which can emit a main peak at 611 nm under the effective excitation of near UV and blue light, the color temperature and color purity are about 1800K and 88%, respectively, making it an excellent red, warm light material [18]. Eu^{3+}-doped $BaLaWO_7$ and $SrLa_2WO_7$ red phosphors were synthesized using the traditional solid-state reaction method [19].

Based on their low phonon energy, outstanding chemical and physical properties, good thermal stability, and strong charge transfer zone in the ultraviolet region, tungstates and molybdates have been widely employed as host materials to phosphors [20,21]. A highly uniform spindle-shaped $SrMoO_4$:Eu^{3+} phosphor was developed, which produces the Eu^{3+} characteristic transition peak $^5D_0$-^7F_J (J = 1, 2, 3, 4) under ultraviolet light excitation (287 nm), with the $^5D_0$-$^7F_2$ transition (613 nm) in the red region being the strongest [22]. The produced $SrMoO_4$:Eu^{3+} phosphors synthesized by Yanan Zhu et al. can be successfully activated by ultraviolet light at 396 nm and emit red light with a prominent peak at 616 nm [23]. Dy^{3+}-doped $SrMoO_4$ nanophosphors were synthesized, which emit blue light at 485 nm and bright yellow light at 576 nm Under UV illumination at 353 nm [24]. $SrWO_4$:Eu^{3+} phosphor was synthesized using the microwave radiation heating approach. The phosphor's excitation spectrum falls in a strong absorption band centered at 295 nm and two weak sharp peaks centered at 389 and 467 nm, and the primary peaks of its emission spectra are positioned at 589 nm and 616 nm [25]. $SrWO_4$:Eu^{3+} phosphors have been successfully synthesized, with the most substantial emission peaks in the emission spectrum at 615 nm under near UV (394 nm) and blue light (450 nm) excitation [26]. The emission intensity of $CaW_{0.4}MoO_4$:Eu^{3+} red phosphor is estimated to be 8.3 times that of $CaWO_4$:Eu^{3+} phosphor [27]. It was discovered that adding Mo(VI) ions to the red phosphor Sr_2ZnWO_6:Eu^{3+} red phosphor significantly increased the emission intensity [28]. The phosphor $Ca_{0.3}Sr_{0.7-1.5y-1.5z}Mo_{1-x}W_xO_4$:$Eu_yLu_z$ was synthesized, and the most incredible emission intensity was observed at x = 0.2, y = 0.1 and z = 0.1 [29]. $Gd_{2(1-x)}Eu_2x(Mo_yW_{1-}yO_4)_3$ phosphors were synthesized, and its highest emission intensities increased with more W(VI) [30]. Despite a significant number of reports on tungstate-molybdate phosphors, there are fewer on $SrMo_{0.5}W_{0.5}O_4$:Eu^{3+}.

This research synthesized the red phosphors $SrWO_4$:Eu^{3+}, $SrMo_{0.5}W_{0.5}O_4$:Eu^{3+}, and $SrMoO_4$:Eu^{3+} using a high-temperature solid-phase technique. Moreover, it examines their spectrum properties as well as the effect of different charge compensators on the luminescence properties of $SrMo_{0.5}W_{0.5}O_4$:Eu^{3+}.

2. Results and Discussion

2.1. Physical and Chemical Phase Analysis

Figure 1 reveals the X-ray powder diffraction (XRD) patterns of (a) $SrMoO_4$, (b) $SrMo_{0.5}W_{0.5}O_4$, and (c) $SrWO_4$ synthesized at different temperatures. Figure 1a shows that the XRD patterns' peak positions and relative intensities of the XRD patterns of the sample $SrMoO_4$ at temperatures of 850 °C, 900 °C, 950 °C, and 1000 °C are essentially the same, which is consistent with the standard card of $SrMoO_4$ (JCPDS 08-0482), indicating that the synthesized samples have a tetragonal crystal system with space group I41/a, and its unit cell data are a = b = 5.3909 Å, c = 12.0118 Å and $\alpha = \beta = \gamma = 90°$. Strontium molybdate can be synthesized at these temperatures without forming an impurity phase. Furthermore, the highest peak intensity was discovered in the sample synthesized at 900 °C, indicating that the crystallinity of the sample is better at this temperature. As a result, the

temperature to synthesize $SrMoO_4$ is set to 900 °C. Figure 1b displays that the XRD patterns' peak positions and relative intensities of the XRD patterns of the sample $SrMo_{0.5}W_{0.5}O_4$ at those temperatures are essentially consistent with the standard card of $SrMoO_4$ (JCPDS 08-0482), demonstrating that the synthesized samples have the structure of $SrMoO_4$, and no new phase is formed. Due to the lanthanide contraction, the atomic and ionic radii of Mo and W, the second and third transition elements in the same group are very close (the atomic radii of Mo and W are both 139 pm, and the ionic radii of Mo(VI) and W(VI) are 59 pm and 60 pm, respectively), and their properties are quite similar. Besides, the structures of ${MoO_4}^{2-}$ and ${WO_4}^{2-}$ are the same. As a result, ${WO_4}^{2-}$ can easily replace ${MoO_4}^{2-}$ to form a solid solution. The peak intensity of the XRD pattern of $SrMo_{0.5}W_{0.5}O_4$ at 900 °C is higher, indicating that the sample's crystallinity is better at this temperature. As a result, 900 °C is the optimal synthesis temperature for $SrMo_{0.5}W_{0.5}O_4$. Figure 1c shows that the XRD patterns of $SrWO_4$ synthesized at temperatures of 850 °C, 900 °C, 950 °C, and 1000 °C are consistent with the standard card of $SrWO_4$ (JCPDS 08-0490), indicating that the synthesized samples have a tetragonal crystal structure with the space group is I41/a (88), and that can synthesize pure phase strontium tungstate at these temperatures. Because the XRD peak of $SrWO_4$ synthesized at 900 °C is the strongest, 900 °C is the best $SrWO_4$ synthesis temperature.

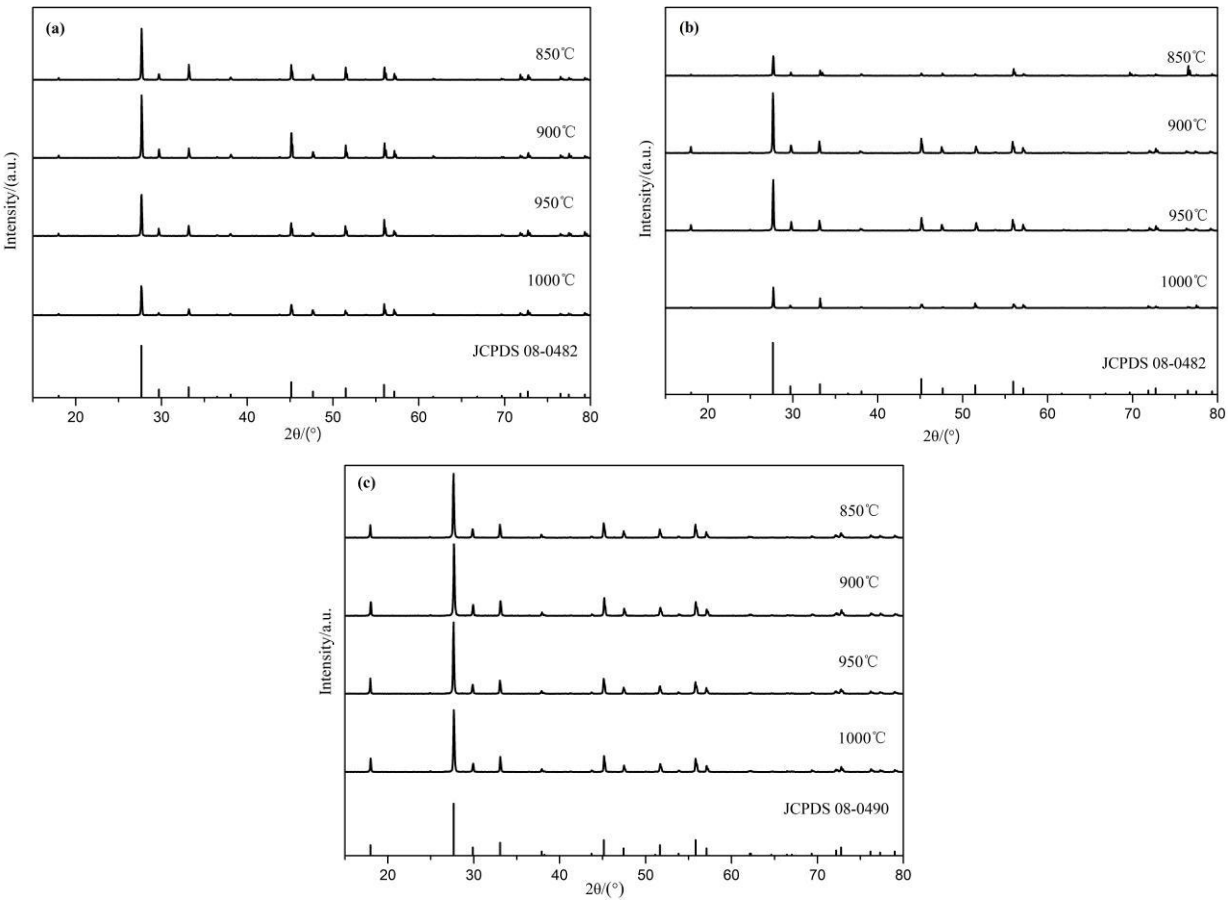

Figure 1. XRD patterns of (**a**) $SrMoO_4$, (**b**) $SrMo_{0.5}W_{0.5}O_4$, (**c**) $SrWO_4$ synthesized at different temperatures.

Figure 2a shows that the diffraction peaks of the $Sr_{1-x}Mo_{0.5}W_{0.5}O_4$:x$Eu^{3+}$ XRD pattern are in line with the standard card #JCPDS 08-0482 ($SrMoO_4$), indicating that the doping of Eu^{3+} in the $SrMo_{0.5}W_{0.5}O_4$ system did not cause phase change and no new phase was created. Rare earth metal Eu and alkaline-earth metal Sr have similar atomic and ionic radii (the atomic radii of Eu and Sr are 208 pm and 215 pm, respectively, while the ionic

radii of Eu^{3+} and Sr^{2+} are 112 pm and 94.7 pm, respectively). When Eu^{3+} is doped into the $SrMo_{0.5}W_{0.5}O_4$ system, it takes the position of Sr^{2+} and creates a continuous solid solution. It has been reported that the O^{2-} is created in the system due to the imbalance in electrovalence as a result of the unequal substitution of Sr^{2+} with Eu^{3+} [23]. According to Figure 2b, the diffraction peaks of the XRD pattern of the phosphor $Sr_{0.99}MoO_4$:0.01Eu^{3+} are compatible with the standard card #JCPDS 08-0482 ($SrMoO_4$), indicating that the sample forms pure phase $SrMoO_4$, and no additional phases are created. That is to say, 1% Eu^{3+} can be added to $SrMoO_4$ without generating a phase shift. As seen in Figure 2c, the diffraction peaks of the XRD pattern of the phosphor $Sr_{0.99}WO_4$:0.01Eu^{3+} are consistent with the standard card #JCPDS 08-0490 ($SrWO_4$), indicating that the pure phase can still be obtained formed by doping 1% Eu^{3+} in $SrWO_4$, and no additional substances form.

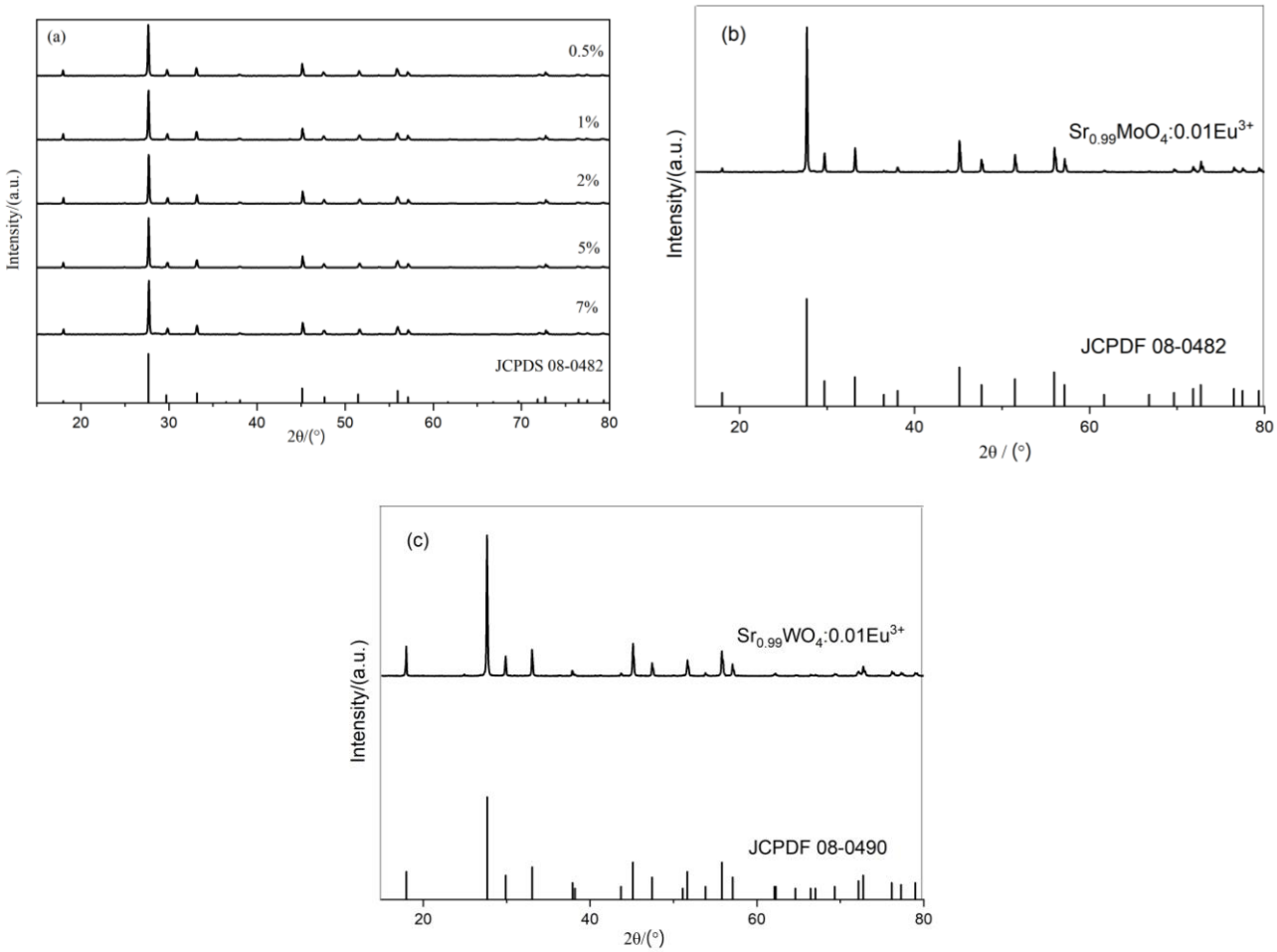

Figure 2. XRD of (**a**) $Sr_{1-x}Mo_{0.5}W_{0.5}O_4$:x$Eu^{3+}$, (**b**) $Sr_{0.99}MoO_4$:0.01Eu^{3+} and (**c**) $Sr_{0.99}WO_4$:0.01Eu^{3+}.

The electrovalent imbalance induced by the unequal substitution of Sr^{2+} with Eu^{3+} in the $Sr_{0.99}Mo_{0.5}W_{0.5}O_4$:0.01$Eu^{3+}$ system can be rectified by adding charge compensators [31]. Figure 3 depicts the XRD patterns of $SrMo_{0.5}W_{0.5}O_4$:Eu^{3+} after doping with various charge compensators. Figure 3 shows that the XRD diffraction peaks of $SrMo_{0.5}W_{0.5}O_4$: Eu^{3+} after adding charge compensator K_2CO_3, Li_2CO_3, Na_2CO_3, NH_4Cl are essentially consistent with the standard card of $SrMoO_4$ (JCPDS 08-0482), that is, there is no charge in the lattice of $SrMo_{0.5}W_{0.5}O_4$:Eu^{3+}, and the phase is still $SrMo_{0.5}W_{0.5}O_4$.

$SrMo_{0.5}W_{0.5}O_4$ has a tetragonal crystal system with a scheelite structure, and each of its units contains one Sr site, one Mo/W site, and four O sites. According to Figure 4, there is only one type of cationic site, Sr, in the lattice, and each, on average, has eight coordinated oxygen ions which include four MoO_4^{2-}/WO_4^{2-} that belong to the S4 symmetry and have no inversion center. Each central W/Mo site is coordinated with four identical O, forming

a MoO_4^{2-}/WO_4^{2-} tetrahedron. As the MoO_4^{2-}/WO_4^{2-} tetrahedral configuration is quite stable, $SrMo_{0.5}W_{0.5}O_4$ retains its lattice structure when Sr^{2+} is replaced by Eu^{3+}.

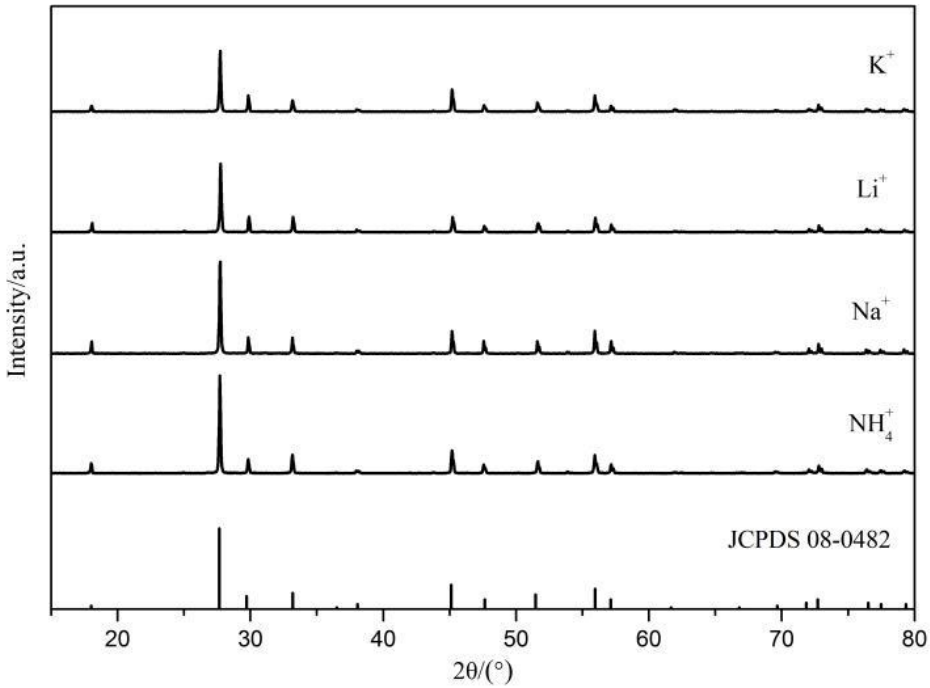

Figure 3. XRD of $Sr_{0.99}Mo_{0.5}W_{0.5}O_4$:0.01$Eu^{3+}$ with different charge compensators.

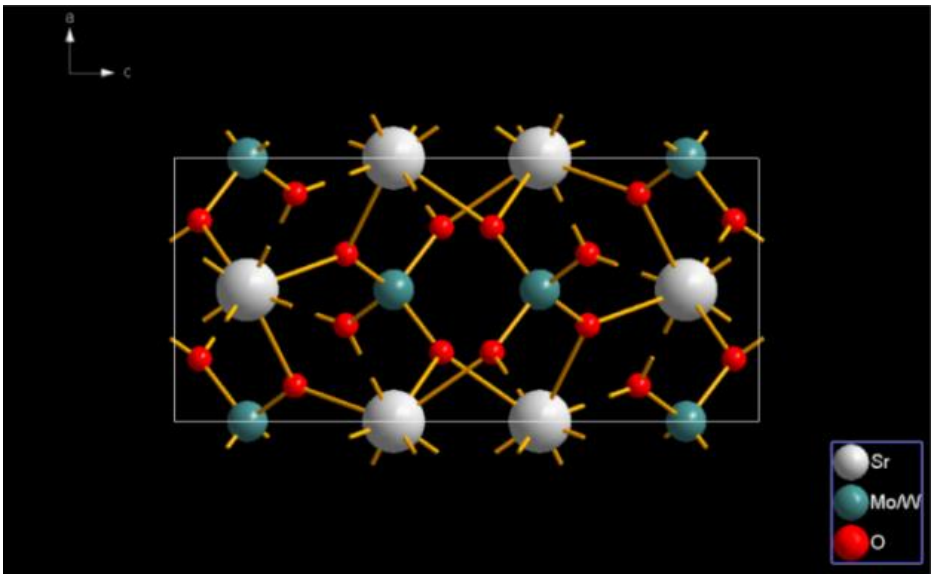

Figure 4. Crystal structure of $SrMo_{0.5}W_{0.5}O_4$.

The FT-IR spectrum of the sample $SrMo_{0.5}W_{0.5}O_4$ was obtained by the KBr pressed disc method. As shown in Figure 5, the FT-IR spectra of the prepared samples have absorption peaks at 818 cm^{-1}, 1630 cm^{-1}, and 3420 cm^{-1}, where the absorption peak at 818 cm^{-1} corresponds to the stretching vibration of O-W/Mo-O, indicating the existence of WO_4^{2-} and MoO_4^{2-} groups in the prepared samples. The absorption peaks at 1630 cm^{-1} and 3420 cm^{-1} are respectively attributed to the bending and stretching vibrations of O-H, causing the water vapor on the surface of the $SrMo_{0.5}W_{0.5}O_4$ surface sample.

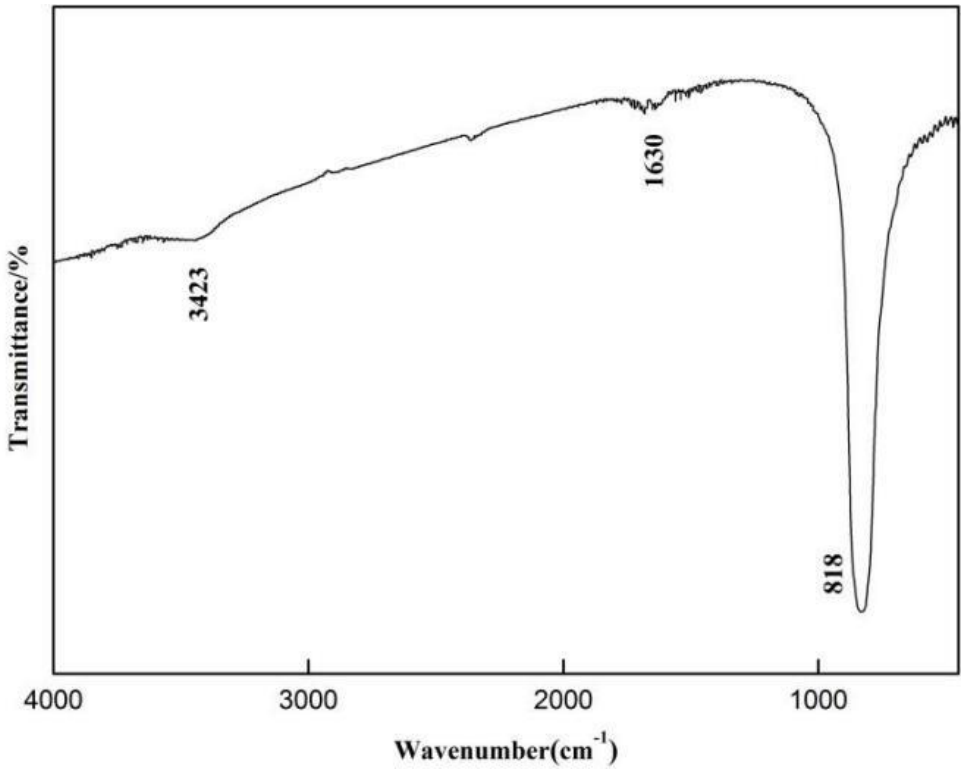

Figure 5. FT-IR spectrum of $SrMo_{0.5}W_{0.5}O_4$ sample.

Figure 6 shows the SEM photos of the phosphor $Sr_{0.99}Mo_{0.5}W_{0.5}O_4$:$Eu^{3+}$ synthesized using a high-temperature solid phase technique at 900 °C. The phosphor $Sr_{0.99}Mo_{0.5}W_{0.5}O_4$:0.01$Eu^{3+}$ has sharp edges and corners, an irregular form, and a particle size of around 2 μm, with agglomeration produced by high-temperature solid-phase preparation.

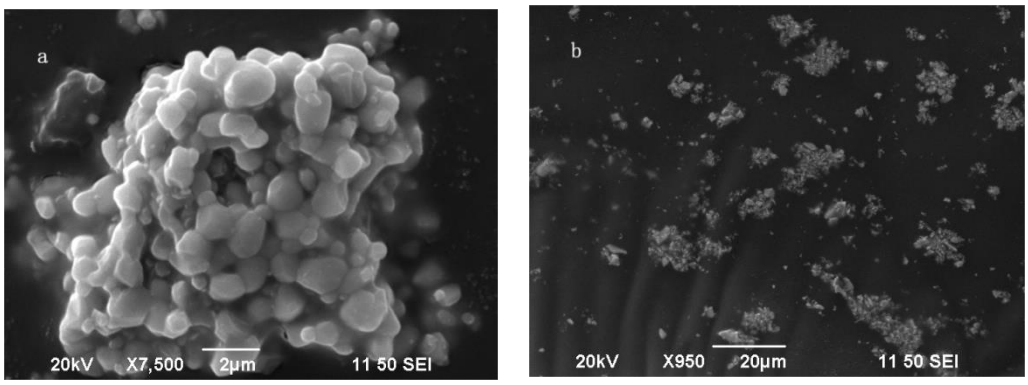

Figure 6. SEM of $Sr_{0.99}Mo_{0.5}W_{0.5}O_4$:$Eu^{3+}$. (**a**) 7500 times; (**b**) 950 times.

2.2. Analysis of Luminescence Performance

Figure 7a–f show the excitation spectra of $SrWO_4$:Eu^{3+}, $SrMo_{0.5}W_{0.5}O_4$: Eu^{3+}, and $SrMoO_4$:Eu^{3+} at 615 nm, and the emission spectra at 273 nm, respectively. Figure 7a,c,e show that the phosphors $SrWO_4$:Eu^{3+}, $SrMo_{0.5}W_{0.5}O_4$: Eu^{3+}, and $SrMoO_4$:Eu^{3+} have a solid and broad CT band in the range of 200 nm to 330 nm, with the center wavelength of 273 nm. Furthermore, the f-f characteristic absorption peaks of Eu^{3+}were also observed at 362 nm ($^7F_0 \rightarrow {}^5D_4$), 378 nm ($^7F_0 \rightarrow {}^5G_2$), 383 nm ($^7F_0 \rightarrow {}^5G_3$), 394 nm ($^7F_0 \rightarrow {}^5L_6$), 416 nm ($^7F_0 \rightarrow {}^5D_3$), 464 nm ($^7F_0 \rightarrow {}^5D_2$) and 534 nm ($^7F_0 \rightarrow {}^5D_1$); the peaks at 273 nm, 394 nm, and 464 nm are stronger, indicating that $SrWO_4$:Eu^{3+}, $SrMo_{0.5}W_{0.5}O_4$: Eu^{3+}, Figure 7b,d,f demonstrate that the emission spectra of $SrWO_4$:Eu^{3+}, $SrMo_{0.5}W_{0.5}O_4$:Eu^{3+}, and $SrMoO_4$:Eu^{3+} are composed

of a succession of sharp fronts, with several emission peaks detected at 568 nm, 591 nm, 615 nm, and 653 nm, corresponding to the $^5D_0 \rightarrow {}^7F_0$, $^5D_0 \rightarrow {}^7F_1$, $^5D_0 \rightarrow {}^7F_2$, $^5D_0 \rightarrow {}^7F_3$ transitions of Eu^{3+}, respectively. When Eu^{3+} ions occupy the matrix's inversion symmetry center site, the magnetic dipole transition of $^5D_0 \rightarrow {}^7F_1$ prevails; conversely, Eu^{3+} ions occupy the matrix's non-inversion symmetry center site, Eu^{3+} electric dipole transition of $^5D_0 \rightarrow {}^7F_2$ dominates. In addition, the red emission peak corresponding to the $^5D_0 \rightarrow {}^7F_2$ transition is the strongest, implying that Eu^{3+} is located in the non-inversion symmetry center lattice site of host lattices of $SrWO_4$:Eu^{3+}, $SrMo_{0.5}W_{0.5}O_4$: Eu^{3+}, and $SrMoO_4$:Eu^{3+}. So $SrMoO_4$:Eu^{3+} can be used as a down converter in UV LEDs and blue light LEDs to achieve red emission.

Figure 8 depicts the emission spectra of $SrWO_4$:0.01Eu^{3+}, $SrMo_{0.5}W_{0.5}O_4$:0.01Eu^{3+}, and $SrMoO_4$:0.01Eu^{3+} under 273 nm monitoring. The emission peak shape and position of Eu^{3+} ions remain constant across all samples. The intensity of the emission increases after the addition of Mo(VI) ions to $SrWO_4$:Eu^{3+} and decreases as Mo(VI) ions totally replace the W(VI), and the emission spectrum of $Sr_{0.99}Mo_{0.5}W_{0.5}O_4$:0.01$Eu^{3+}$ is the strongest. The reason for that is: the introduction of Mo(VI) ions will form MoO_4^{2-} groups, which can efficiently modulate the diversity of the Eu^{3+} surrounding environment and shift the symmetry of the local crystal field, thereby promoting the charge transfer transition of $O^{2-} \rightarrow Eu^{3+}$, the Eu^{3+} hypersensitive transition, and the electron-migration energy of MoO_4^{2-} (M = W, Mo) in the matrix to transfer to Eu^{3+} [32]. Furthermore, after introducing Mo(VI), the average distance between WO_4 groups becomes wider [27], leading to a lower energy transfer between WO_4 groups and then more incident energy will be transferred to Eu^{3+}. When the Mo(VI) ion concentration is too high, the impact of the ion-pair interaction between Eu^{3+} ions will be increased, leading to a reduction in the phosphor's luminous efficiency [33]. Therefore, inserting Mo(VI) can effectively improve the luminous properties of $SrWO_4$:Eu^{3+} phosphors.

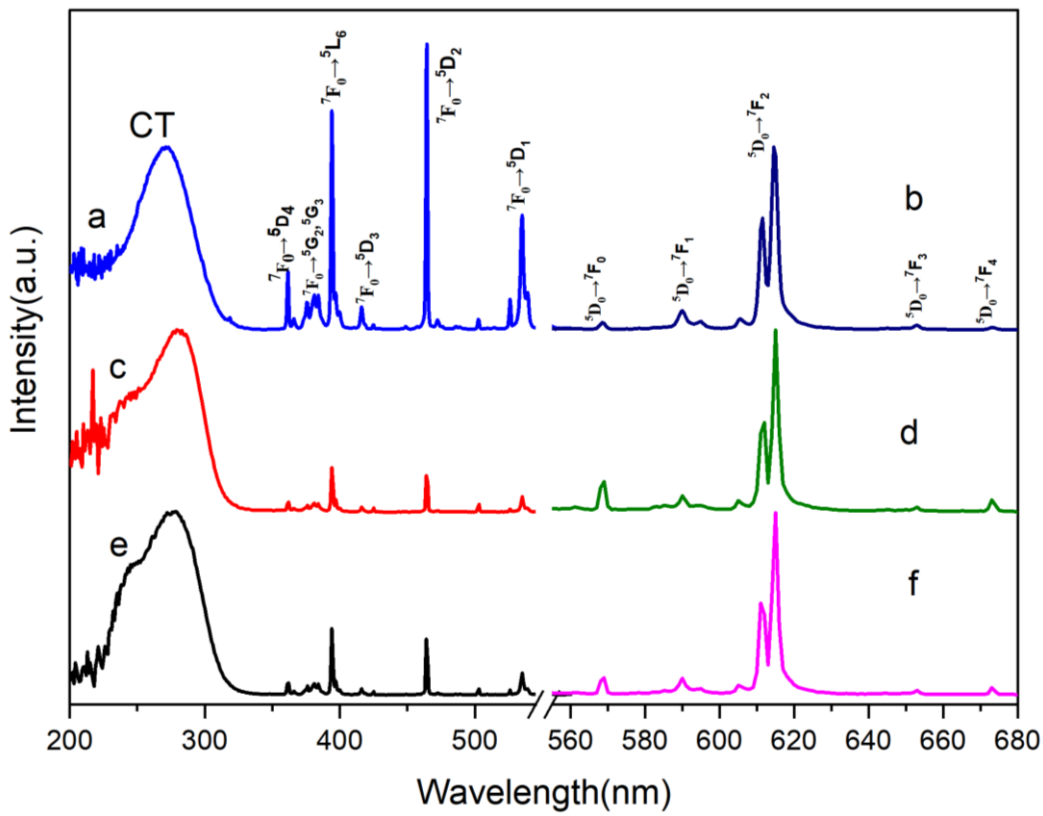

Figure 7. Excitation (**a**,**c**,**e**) and emission (**b**,**d**,**f**) spectra of $SrWO_4$:Eu^{3+}, $SrMo_{0.5}W_{0.5}O_4$: Eu^{3+}, and $SrMoO_4$:Eu^{3+}.

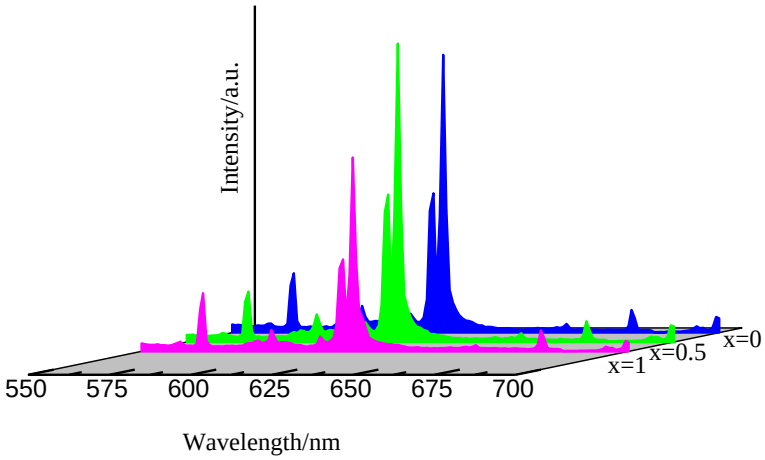

Figure 8. The emission spectrum of $Sr_{0.99}Mo_xW_{1-x}O_4$:0.01Eu^{3+}(x = 0, 0.5, 1).

Figure 9a depicts the emission spectra of $SrMo_{0.5}W_{0.5}O_4$:Eu^{3+} with varying Eu^{3+} concentrations excited at 273 nm. Figure 9a shows that all samples' peak forms and positions remain constant. However, with the Eu^{3+} concentration increasing, the luminescence intensity first increases and then decreases. The emission peak intensity of $Sr_{0.99}Mo_{0.5}W_{0.5}O_4$:0.01$Eu^{3+}$ achieves its maximum when the doping concentration of Eu^{3+} is 1%, and if the concentration of Eu^{3+} continues to increase, the phenomenon of concentration quenching appears. This is because although the transition of emitted light increases with the increase of the Eu^{3+} concentration, which can effectively improve the intensity of the emitted light, the continuous increase of the doping amount of Eu^{3+} will narrow the distance between Eu^{3+}, resulting in a decrease in emission intensity due to nonradiative energy transfer between Eu^{3+}. To look into the energy transfer of Eu^{3+} ions in $SrMo_{0.5}W_{0.5}O_4$, the critical distance of Eu^{3+} ions is first estimated using the formula below.

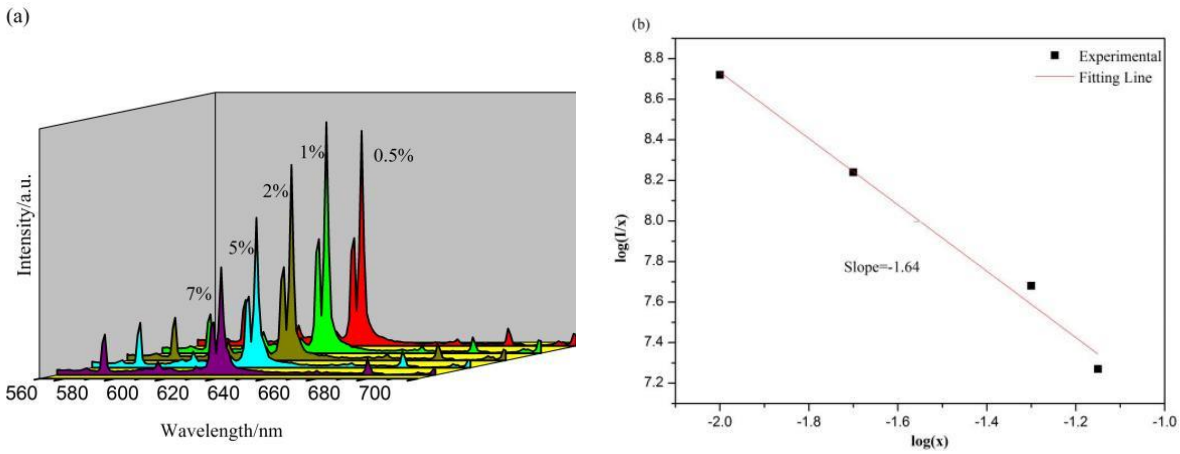

Figure 9. (**a**) The emission spectrum of $Sr_{1-y}Mo_{0.5}W_{0.5}O_4$:y$Eu^{3+}$(y = 0.005, 0.01, 0.02, 0.05, 0.07), (**b**) Dependence of log (I/x) on log (x) for $Sr_{1y}Mo_{0.5}W_{0.5}O_4$:y$Eu^{3+}$.

The critical distance R_c can be computed using the Blass theory formula [34]:

$$R_c = 2\left(\frac{3V}{4\pi x_{cN}}\right)$$

In this equation, V denotes the unit cell volume, X_c is the critical concentration of Eu^{3+} in $SrMo_{0.5}W_{0.5}O_4$(the optimal doping concentration), and N denotes the number of cations per unit cell of $SrMo_{0.5}W_{0.5}O_4$ crystal. Figure 9a shows the critical threshold concentration of Eu^{3+} is 0.01 in $SrMo_{0.5}W_{0.5}O_4$ crystal, N = 4, V = 349.78 $Å^3$. According

to the Blass formula, R_c = 25.57 Å. In general, non-radiative energy transfer modes are broadly classified as electron exchange interaction and electric multipole interaction. When the critical distance R_c is around 5 Å, the non-radiative energy transfer mode is electron exchange interaction. When R_c reaches 25.57 Å, much more than 5 Å, the energy transfer between Eu^{3+} in $SrMo_{0.5}W_{0.5}O_4$: Eu^{3+} is electric multipolar interaction.

The energy transfer formula for the electric multipole interaction can be derived using Van Uitert's theory [35]:

$$\frac{I}{X} = K\left[1 + \beta(X)^{\frac{\theta}{3}}\right]^{-1}$$

In this formula, I is the integrated emission intensity, X is the activator concentration above the critical concentration, and K and β are constants for a given matrix. Analyzing the constant θ confirms the energy transfer mode of the electric multipole interaction, and the number of cations in the unit cell of $SrMo_{0.5}W_{0.5}O_4$ crystal can be deduced. θ = 6, 8, and 10 correspond to dipole-dipole (d-d), dipole-quaternary (d-q), and quaternary-quaternary (q-q) interactions, respectively. Figure 9b reveals the connection between log(I/X) and log(X) of $SrMo_{0.5}W_{0.5}O_4$: Eu^{3+}. If the slope –1.64 is –θ/3, then θ will be 4.92, which the value is closer to 6. As a result, the electric dipole-electric dipole (d-d) interaction causes the quenching concentration in $Sr_{1-x}Mo_{0.5}W_{0.5}O_4$:x$Eu^{3+}$.

The partial substitution of Sr^{2+} by Eu^{3+} in $SrMo_{0.5}W_{0.5}O_4$:Eu^{3+} will result in a charge imbalance, leading to excessive charge defects in the lattice and thus decreasing the phosphor luminous efficiency. However, adding the right amount of good charge compensator can increase the sample's luminous efficiency [31]. Figure 10 depicts the emission spectra of phosphors $SrMo_{0.5}W_{0.5}O_4$: Eu^{3+}, M (M = K^+, Li^+, Na^+, NH_4^+) doped with various charge compensators. The addition of the charge compensator doesn't modify the position of the emission peak of $SrMo_{0.5}W_{0.5}O_4$: Eu^{3+}. Various charge compensators have different effects on the luminescence intensity of $SrMo_{0.5}W_{0.5}O_4$:Eu^{3+}, but their doping will improve the luminescence intensity, with NH_4^+ having the best effect.

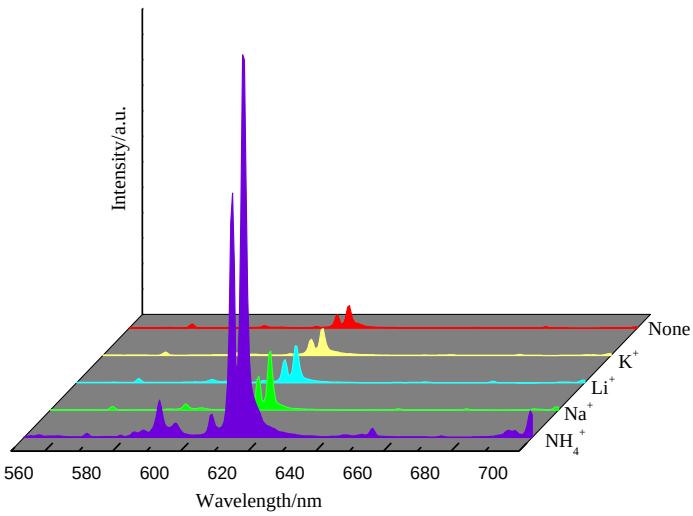

Figure 10. Emission spectra of $SrMo_{0.5}W_{0.5}O_4$:Eu^{3+} with different charge compensators.

Figure 11 depicts the luminescence intensity of $Sr_{0.99}Mo_{0.5}W_{0.5}O_4$:0.01$Eu^{3+}$ at various NH_4^+ doping concentrations (0%, 3%, 6%, 10%, 15%). The figure shows that when the concentration of NH_4^+ is low, the luminescence intensity of the sample increases as the concentration of NH_4^+ increases. The sample's emission peak intensity reaches its maximum highest when the NH_4^+ doping concentration is 3%. As the concentration of NH_4^+ continues to increase, concentration quenching will occur. This is due to the fact that when the concentration of NH_4^+ is low, NH_4^+ can replace the position of Sr^{2+} in the lattice, lowering the symmetry of the lattice and modifying the local crystal field environment around Eu^{3+}, which eventually increases the sample's luminescence performance [36,37];

At the same time, due to the difference in the quantities of electric charges of NH_4^+ and Sr^{3+}, oxygen vacancies will be formed after replacing Sr^{2+} in order to maintain the electrical neutrality of NH_4^+. These oxygen vacancies can transfer charge with Eu^{3+} [34], thereby increasing the sample's luminescence intensity. On the other hand, the excess NH_4^+ will enter the lattice gaps and induce lattice distortions, affecting the luminescence intensity of the samples.

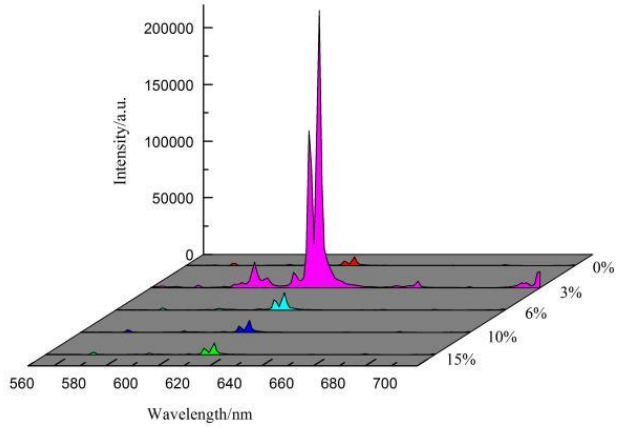

Figure 11. Emission spectra of $SrMo_{0.5}W_{0.5}O_4$:Eu^{3+} with different concentrations of NH_4^+.

Figure 12 shows the luminescence decay curves of $SrMo_{0.5}W_{0.5}O_4$:Eu^{3+} phosphors doped with several charge compensators (K^+, Li^+, Na^+, NH_4^+) at an excitation wavelength of 464 nm and an emission wavelength of 615 nm. As illustrated in Figure 12, the decay curves of all samples' emitted light satisfy a bi-exponential equation [38]:

$$I(t) = I_0 + A_1 \exp\left(\frac{-t}{\tau_1}\right) + A_2 \exp\left(\frac{-t}{\tau_2}\right)$$

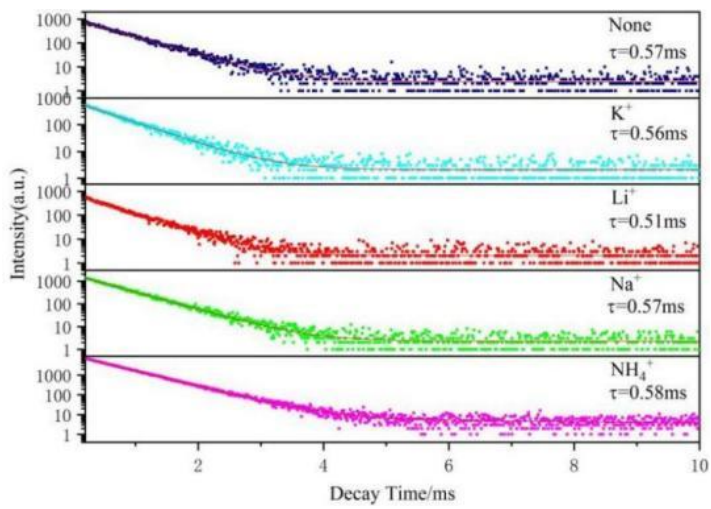

Figure 12. Lifetime decay curve of $SrMo_{0.5}W_{0.5}O_4$:0.01Eu^{3+}, A (A = Li^+, Na^+, K^+, NH_4^+).

In the formula, I(t) denotes the emission intensity at time t, I_0 represents the initial emission intensity, A_1 and A_2 are the pre-exponential factors of each decay component, and τ_1 and τ_2 are the decay times of each component. The average emission decay time (τ_{ave}) can be calculated using the below [38].

$$\tau_{ave} = \frac{A_1\tau_1^2 + A_2\tau_2^2}{A_1\tau_1 + A_2\tau_2}$$

The average emission decay time τ_{ave} shown in Figure 12, was calculated to be 0.57 ms for $Sr_{0.99}Mo_{0.5}W_{0.5}O_4$:0.01$Eu^{3+}$ and 0.0.51, 0.0.57, 0.56, and 0.0.58 ms for $Sr_{0.99}Mo_{0.5}W_{0.5}O_4$:0.01$Eu^{3+}$, A (A = Li^+, Na^+, K^+, NH_4^+), respectively. The emission decay times of all ceramic samples were very similar and slightly lower than that of the powder sample. This suggests that, in the ceramic samples, the electronic relaxation time from the split $^5D_2$ energy levels to the lowest transition energy level $^5D_0$ was reduced. When the charge compensator NH_4^+ concentration is 3% in the $Sr_{0.99}Mo_{0.5}W_{0.5}O_4$:0.01$Eu^{3+}$, A (A = K^+, Li^+, Na^+, NH_4^+) system, the fluorescence lifespan of the sample achieves a maximum of 0.58ms. It is also demonstrated that adding NH_4^+ can significantly improve the luminescent characteristics of the samples.

Figure 13 depicts the color coordinates of samples $Sr_{0.99}Mo_{0.5}W_{0.5}O_4$: 0.01$Eu^{3+}$ (b), $Sr_{0.99}Mo_{0.5}W_{0.5}O_4$: 0.01$Eu^{3+}$, 0.03$NH_4^+$ (c), where the color coordinates of b (0.642, 0.358) and c (0.656, 0.343) are both positioned at the edge of the red area, indicating that the synthetic samples have a high color purity. The color coordinates of the $SrMo_{0.5}W_{0.5}O_4$: Eu^{3+} sample show a red-shifted after adding the charge compensator NH_4^+, demonstrating that NH_4^+ can successfully improve the luminescence properties of the non-$SrMo_{0.5}W_{0.5}O_4$: Eu^{3+} sample. The coordinates are close to the ideal red light's coordinates (0.670, 0.333) (d) and better than the commercial red phosphor Y_2O_2S:Eu^{2+}'s coordinates (0.622, 0.351) (a).

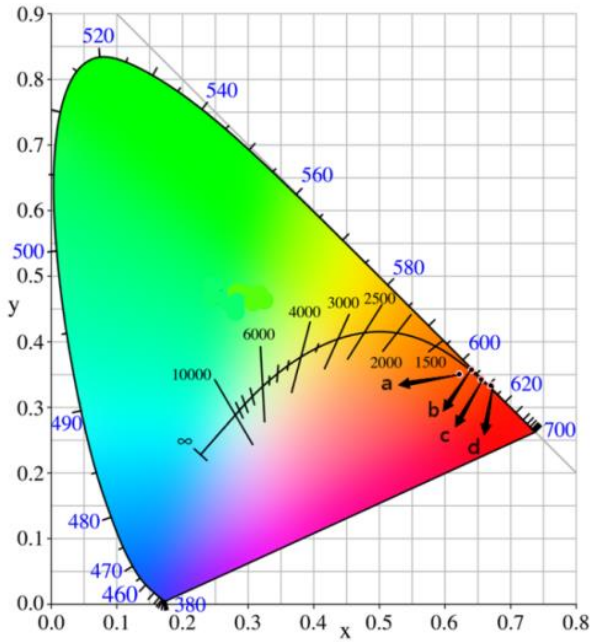

Figure 13. CIE color coordinates of Y_2O_2S:Eu^{2+} (**a**), $Sr_{0.99-x}Mo_{0.5}W_{0.5}O_4$:0.01$Eu^{3+}$ (**b**), $Sr_{0.99}Mo_{0.5}W_{0.5}O_4$:0.01$Eu^{3+}$, 0.03$NH_4^+$ (**c**) and ideal red light (**d**).

3. Materials and Methods

3.1. Sample Preparation

All samples were synthesized in an air atmosphere using a high-temperature solid phase method. The raw materials included $SrCO_3$(A.R.), MoO_3(A.R.), WO_3(A.R.), Eu_2O_3 (99.99%), Na_2CO_3 (A.R.), Li_2CO_3(A.R.), K_2CO_3 (A.R.), and NH_4Cl (A.R.). They were accurately weighed based on the stoichiometric ratio of $Sr_{(1-y)}Mo_xW_{1-x}O_4$:yEu^{3+}, transferred to an agate mortar, added a tiny amount of anhydrous ethanol, ground for 30 min, then transferred the blended powder was to a high-temperature furnace and calcined at a certain temperature for 5 h.

3.2. Sample Testing and Characterization

The structures of the samples were studied using a Bruker (Billerica, MA, USA) AXS D8 X-ray diffractometer (XRD), with Cu Kα lines as a radiation source. An operating

voltage of 40 KV, An operating current of 30 mA, and a scanning range of 2θ = 15–80°; the microscopic morphology of the samples was characterized using a JSM-6490LV scanning electron microscope (SEM). The sample's Fourier transform infrared (FT-IR) spectra were evaluated by a Perkin Elmer(Norwalk, CT, USA) Type NicoLet670-shaped Fourier transform infrared spectrometer using the KBr pressed-disc technique and a resolution of 4 cm^{-1}. The excitation, and emission spectra, luminescence decay curves of the luminous material were evaluated using an Edinburgh FS5 fluorescence spectrometer equipped with a 150 W xenon lamp as an excitation light source. All of the preceding experiments were carried out at room temperature.

4. Conclusions

The phosphor $SrMo_{0.5}W_{0.5}O_4$: Eu^{3+} synthesized by the high-temperature solid-phase technique has an optimal synthesis temperature of 900 °C. The phosphor possesses a tetragonal crystal structure, and the doping of Eu^{3+} does not affect the crystal phase. The phosphor's Fourier infrared spectrum indicates a stretching vibration of O-W/Mo-O; the SEM shows irregular particles with sharp edges and corners, a particle size of 2 μm, and numerous agglomerations. The primary excitation peaks of the phosphor $SrMo_{0.5}W_{0.5}O_4$: Eu^{3+} are positioned at 273 nm, 397 nm, and 464 nm, respectively, and are attributable to the charge migration of $O^{2-}\rightarrow Eu^{3+}$ and the distinctive spectrum of Eu^{3+} ($^7F_0\rightarrow{}^5L_6$, $^7F_0\rightarrow{}^5D_2$). The central light peak of the emitted light is around 615 nm, representing a possible red fluorescent material that can be used as a down converter in UV LEDs and blue light LEDs. When the emission spectra of red phosphors $SrWO_4$:Eu^{3+}, $SrMo_{0.5}W_{0.5}O_4$: Eu^{3+}, and $SrMoO_4$:Eu^{3+} are compared, it is discovered that after the introduction of Mo(VI) into $SrWO_4$:Eu^{3+}, the emission intensity increases and when Mo(VI) ions completely replace the W(VI), the emission intensity decreases. The optimal doping concentration (quenching concentration)of Eu^{3+} in $SrMo_{0.5}W_{0.5}O_4$: Eu^{3+} is 1%, and the quenching concentration is 1%, which is due to the galvanic-even-order interaction in the electric multilevel interaction, and its critical distance is R_c = 25.57 Å. Charge compensators of various types, including Eu^{3+}: K^+, Li^+, Na^+, and NH_4^+, were added into $SrMo_{0.5}W_{0.5}O_4$, with NH_4^+ having the best effect and the best doping concentration of it being 3%. In comparison to the color coordinates (0.642, 0.358) of $SrMo_{0.5}W_{0.5}O_4$: Eu^{3+}, the color coordinates (0.656, 0.343) of $SrMo_{0.5}W_{0.5}O_4$: Eu^{3+}, NH_4^+ exhibit an apparent red shift phenomenon, and the color coordinates of the obtained phosphors are all better than the color coordinates of commercial red phosphors (0.622, 0.351) and are closer to the ideal.

Author Contributions: Methodology, L.K.; software, Y.N. and H.Y.; formal analysis, L.K. and H.Y.; investigation, S.Z.; resources, R.W. and Q.D.; data curation, H.S.; writing—original draft preparation, H.S.; writing—review and editing, L.K.; visualization, Y.Y.; supervision, G.L.; project administration, L.K.; funding acquisition, H.Y. All authors have read and agreed to the published version of the manuscript.

Funding: Jilin Province Specialized Science Foundation for Youths (No. YDZJ202101ZYTS163).

Institutional Review Board Statement: Not applicable.

Informed Consent Statement: Not applicable.

Data Availability Statement: The data presented in this study are available on request from the corresponding author.

Acknowledgments: This work was financially supported by Jilin Province Specialized Science Foundation for Youths (No. YDZJ202101ZYTS163). The data were obtained using equipment maintained by the Jilin Insititute of Chemical Technology Center of Characterization and Analysis.

Conflicts of Interest: The authors declare no conflict of interest.

Sample Availability: Samples of the compounds are not available from the authors.

References

1. Yang, S.; Jiang, B.; Wu, J.H.; Duan, C.G.; Shan, Y.K.; Zhao, Q.B. $LaMoBO_6$:Tb^{3+},Eu^{3+}/Sm^{3+},Bi^{3+} yellow phosphors with exceptionally high quantum yields that can be excited by blue light. *J. Mater. Chem. C* **2021**, *9*, 7065–7073. [CrossRef]
2. Yi, L.H.; Zhou, L.Y.; Wang, Z.L.; Sun, J.H.; Gong, F.Z.; Wan, W.; Wang, W. KGd $(MoO_4)_2$:Eu^{3+} as a promising red phosphor for light-emitting diode application. *Curr. Appl. Phys.* **2010**, *10*, 208–213. [CrossRef]
3. Sokolnicki, J. Nitridated $CaSiO_3$:Eu and $SrSiO_3$:Eu phosphors for LEDs. *J. Alloy. Compd.* **2022**, *903*, 163973–163980. [CrossRef]
4. Kong, L.; Liu, Y.Y.; Dong, L.P.; Zhang, L.; Qiao, L.; Wang, W.S.; You, H.P. Enhanced red luminescence in $CaAl_{12}O_{19}$: Mn^{4+}via doping Ga^{3+} for plant growth lighting. *Dalton Trans.* **2020**, *49*, 1947–1954. [CrossRef]
5. Nakamura, S.; Fasol, G. *The Blue Laser Diode: GaN Based Light Emitters and Lasers*; Springer: Berlin/Heidelberg, Germany, 1996; pp. 1–24.
6. Gao, R.P.; Liang, H.; Chen, T.; Wu, Z.Y.; Jiang, Z.Y.; Yi, X.H.; Wen, J.P.; Zhong, Q.H. Study on luminescence characterizations of $SrMg_2La_2W_2O_{12}$:Eu^{3+} red-emitting phosphor. *J. Phys. Chem. Solids* **2022**, *163*, 110569–110577.
7. Qin, L.; Chen, J.H.; Chen, X.M.; Shao, H.B.; Wang, Z.L. Photoluminescence, thermal stability and structural properties of red-emitting phosphors $Na_5YSi_4O_{12}$:Eu^{3+}. *J. Lumin.* **2021**, *238*, 118228–118233. [CrossRef]
8. Kachou, I.; Saidi, K.; Salhi, R.; Dammak, M. Synthesis and optical spectroscopy of $Na_3Y(VO_4)_2$:Eu^{3+}phosphors for thermometry and display applications. *Rsc. Adv.* **2022**, *12*, 7529–7539. [CrossRef]
9. Matsumoto, S.; Watanable, T.; Ito, A. Photoand Radioluminescence Properties of Eu^{3+}-doped Y_2O_3 Thick Film Phosphor Prepared via Chemical Vapor Deposition. *Sens. Mater.* **2022**, *34*, 669–675.
10. Chen, F.; Akram, M.N.; Chen, X.Y. Improved photoluminescence performance of Eu^{3+}-doped $Y_2(MoO_4)_3$ red-emitting phosphor via orderly arrangement of the crystal lattice. *Molecules* **2023**, *28*, 1014. [CrossRef]
11. Dikhtyar, Y.Y.; Spassky, D.A.; Morozov, V.A.; Polyakov, S.N.; Romanova, V.D.; Stefanovich, S.Y.; Deyneko, D.V.; Baryshnikova, O.V.; Nikiforov, I.V.; Lazoryak, B.I. New series of red-light phosphor $Ca_{9-x}Zn_xGd_{0.9}(PO_4)_7$:0.1$Eu^{3+}$ (x = 0–1). *Molecules* **2023**, *28*, 352. [CrossRef]
12. Huong, T.T.; VinhLe, T.; Hoang, T.K.; Le, D.T.; Nguyen, D.V.; Do, T.T.; Ha, T.P. Synthesis and in vitro testing of YVO_4:Eu^{3+}@silica-NH-GDA-IgG bio-nano complexes for labelling MCF-7 breast cancer cells. *Molecules* **2023**, *28*, 280. [CrossRef] [PubMed]
13. Gontcharenko, V.E.; Kiskin, M.A.; Dolzhenko, V.D.; Korshunov, V.M.; Taydakov, I.V.; Belousov, Y.A. Mono- and mixed metal complexes of Eu^{3+}, Gd^{3+}, and Tb^{3+} with a diketone, bearing pyrazole moiety and CHF_2-group: Structure, color tuning, and kinetics of energy transfer between lanthanide ions. *Molecules* **2021**, *26*, 2655. [CrossRef]
14. Kolesnikov, I.E.; Daria, V.; Mamonova, M.A.; Kurochkin, E.Y.; Kolesnikov, E.L. Optical thermometry by monitoring dual emissions from YVO_4 and Eu^{3+} in YVO_4:Eu^{3+} nanoparticles. *ACS Appl. Nano Mater.* **2021**, *4*, 1959–1966. [CrossRef]
15. Li, J.J.; Liu, X.H.; Liu, Y.F. Luminescence investigation of a novel red-emitting Sr_3NaSbO_6:Eu^{3+} phosphor. *Optik* **2021**, *242*, 166809–166816. [CrossRef]
16. Chen, S.M.; Zeng, Q.; Guo, C.C.; Liu, L.; Yao, C.F.; Chen, X.; Feng, Y.Z. Sol-gel preparation and luminescent properties of $Li_{2.06}Nb_{0.18}Ti_{0.\ 6}O_3$: Eu^{3+} red phosphor. *Optik* **2021**, *241*, 166921–166927. [CrossRef]
17. Zhang, Y.; Dong, Y.Y.; Xu, J.Y.; Wei, B. Ge^{4+} Eu^{3+}-codoped Y_2SiO_5 as a novel red phosphor for white LED applications. *Phys. Status Solidi A* **2017**, *214*, 1600731. [CrossRef]
18. Yu, B.; Li, Y.C.; Zhan, R.P.; Li, H.; Wang, Y.N. A novel thermally stable eulytite-type $NaBaBi_2(PO_4)_3$:Eu^{3+} red-emitting phosphor for pc-WLEDs. *J. Alloy. Compd.* **2021**, *852*, 157020–157032. [CrossRef]
19. Wei, D.L.; Hyo, J.S.; Liu, Y.S.; Yang, X.F. Reveal luminescence differences via comparative studies of dynamic spectra in Eu^{3+}-activated $BaLa_2WO_7$ and $SrLa_2WO_7$ phosphors. *Ceram. Int.* **2023**, *49*, 7534–7545.
20. Huang, X.Y.; Li, B.; Guo, H. Highly efficient Eu^{3+}-activated $K_2Gd(WO_4)(PO_4)$ red-emitting phosphors with superior thermal stability for solid-state lighting. *Ceram. Int.* **2017**, *43*, 10566–10571. [CrossRef]
21. Du, P.; Wang, L.L.; Yu, J.S. Luminescence properties and energy transfer behavior of single-component $NaY(WO_4)_2$: Tm^{3+}/Dy^{3+}/Eu^{3+} phosphors for ultraviolet-excited white light-emitting diodes. *J. Alloy. Compd.* **2016**, *673*, 426–432. [CrossRef]
22. Ren, X.L.; Zhang, Y.; Li, Q.Y.; Yu, M. Sodium citrate (Na_3Cit)-assisted hydrothermal synthesis of uniform spindle-like $SrMoO_4$:Eu^{3+}phosphors. *Mater. Res. Bull.* **2014**, *59*, 283–289. [CrossRef]
23. Zhu, Y.N.; Zheng, G.H.; Dai, Z.X.; Zhang, L.Y.; Mu, J.J. Core-Shell Structure and Luminescence of $SrMoO_4$:Eu^{3+}(10%) Phosphors. *J. Mater. Sci. Technol.* **2016**, *32*, 1361–1371. [CrossRef]
24. Chavan, A.B.; Gawande, A.B.; Gaikwad, V.B.; Jain, G.H.; Deore, M.K. Hydrothermal synthesis and luminescence properties of Dy^{3+} doped $SrMoO_4$ nano-phosph. *J. Lumin.* **2021**, *234*, 117996–118003. [CrossRef]
25. Feng, H.; Yang, Y.; Wang, X. Microwave radiation heating synthesis and luminescence of $SrWO_4$ and $SrWO_4$:xEu^{3+} powders. *Ceram. Int.* **2014**, *40*, 10115–10118. [CrossRef]
26. Saravanakumar, S.; Sivaganesh, D.; Sivakumar, V.; Sasikumar, S.; Thirumalaisamy, T.K. Red emitting Eu^{3+}induced $SrWO_4$ materials: Synthesis, structural, morphological and photoluminescence analysis. *Phys. Scr.* **2021**, *96*, 125817–125832. [CrossRef]
27. Huang, X.Y.; Li, B.; Guo, H.; Chen, D.Q. Molybdenum-doping-induced photoluminescence enhancement in Eu^{3+} activated $CaWO_4$ red-emitting phosphors for white light-emitting diodes. *Dyes. Pigmen.* **2017**, *143*, 86–94. [CrossRef]
28. Li, L.; Pan, Y.; Zhou, X.J.; Zhao, C.L.; Wang, Y.J.; Jiang, S.; Suchocki, A.; Brik, M.G. Luminescence enhancement in the $Sr_2ZnW_{1-x}Mo_xO_6$:Eu^{3+},Li^+ phosphor for near ultraviolet based solid state lighting. *J. Alloy. Compd.* **2016**, *685*, 917–926. [CrossRef]

29. Xie, H.D.; Chen, C.; Li, J.; He, Y.Y.; Wang, N. Sol-gel synthesis and luminescent performance of Eu^{3+}, Lu^{3+}co-doped $Ca_{0.3}Sr_{0.7}Mo_{1-x}W_xO_4$ red-emitting phosphor. *Inorg. Nano Met. Chem.* **2020**, *51*, 1297–1305. [CrossRef]
30. Zhang, M.; Cao, C.Y.; Chen, X.T.; Chen, Z.J.; Yang, L.; Li, Y.C.; Xie, A. Synthesis, luminescent properties, and thermal stabilities of $Gd_{2(1-x)}Eu_{2x}(Mo_yW_{1-y}O_4)_{(3)}(0 \leq x \leq 0.2, 0 \leq y \leq 1)$ solid solution phosphors. *Solid State Sci.* **2021**, *120*, 106710–106719. [CrossRef]
31. Liu, S.Q.; Liang, Y.J.; Zhu, Y.L.; Li, H.R.; Chen, J.H.; Wang, M.Y.; Li, W.J. Enhancing emission intensity and thermal stability by charge compensation in $Sr_2Mg_3P_4O_{15}$:Eu^{3+}. *J. Am. Ceram. Soc.* **2018**, *101*, 1655–1664. [CrossRef]
32. Yang, C.G.; Huang, Q.M.; Lin, G.Q. Structure and luminescence properties of $Eu^{3+}/Tb^{3+}/MoO_4{}^{2-}$ tri-doped calcium tungstate phosphors. *J. Chin. Ceram. Soc.* **2015**, *43*, 75–80. (In Chinese)
33. Chiu, C.H.; Wang, M.F.; Lee, C.S.; Chen, T.M. Structural, spectroscopic and photoluminescence studies of $LiEu(WO_4)_{2-x}$ $(MoO_4)_x$ as a near-UV convertible phosphor. *J. Solid State Chem.* **2006**, *180*, 619–627. [CrossRef]
34. Blasse, G. Energy transfer in oxidicphosphors. *Philips. Res. Rep.* **1969**, *24*, 131–136.
35. Van Uitert, L.G. Characterization of energy transfer interactions between rare earth ions. *J. Electrochem. Soc.* **1967**, *114*, 1048–1053. [CrossRef]
36. Grzyb, T.; Lis, S. Structural and spectroscopic properties of LaOF:Eu^{3+} nanocrystals prepared by the sol–gel Pechini method. *Inorg. Chem.* **2011**, *50*, 8112–8120. [CrossRef] [PubMed]
37. Chen, G.Y.; Liu, H.C.; Somesfalean, Q.; Sheng, G.Y.; Liang, H.J.; Zhang, Z.G.; Sun, Q.; Wang, F.P. Enhancement of the upconversion radiation in Y_2O_3:Er^{3+} nanocrystals by codoping with Li^+ ions. *Appl. Phys. Lett.* **2008**, *92*, 139. [CrossRef]
38. Blasse, G.; Grabmarier, B.C. *Luminescent Materials*; Springer: Berlin/Heidelberg, Germany, 1994; p. 46.